This article has been accepted for publication in IEEE Transactions on Antennas and Propagation. This is the author's version which has not been fully edited and content may change prior to final publication. Citation information: DOI 10.1109/TAP.2023.3322198

Differentially Fed Dual-Band Base Station Antenna with Multimode Resonance and High Selectivity for 5G Applications

Xuekang Liu, Benito Sanz-Izquierdo, Haiwei Zhang, Steven Gao, *Fellow, IEEE*, Wei Hu, *Senior Member, IEEE*, Xue-Xia Yang, *Senior Member, IEEE*, Josaphat Tetuko Sri Sumantyo

***Abstract*—A dual-polarized antenna with multimode resonance and high selectivity is proposed in this paper to cover the 5G sub-6 GHz bands. The proposed antenna achieves dual wide impedance bandwidth characteristics by incorporating a dual mode coupled patch and four planar coupled strips around the driven patch. Through the four resonant modes of these structures, the antenna effectively covers the two desired frequency bands. Moreover, the electric/magnetic coupling between the driven patch, dual mode coupled patch, and planar coupled strips enables the creation of three radiation nulls that suppress unwanted radiation. To further improve the out-of-band rejection level and half power beamwidth, four shorted strips are introduced around the radiator. The introduction of these strips results in a 4th radiation null at higher out-of-band frequencies and expands the antenna's half power beamwidth from 52° to 62°. To demonstrate the feasibility of the design, both the proposed antenna and its array were manufactured and tested. Measured results show that the filtering element was able to operate within frequency bands of 3.24-3.83 GHz (16.7%) and 4.74-5.30 GHz (11.2%) with a reference of $|S_{dd11}| < -14$ dB. The input ports exhibited a high level of isolation, measuring 40 dB. Furthermore, the four radiation nulls proved effective in suppressing out-of-band radiation.**

***Index Terms*—Base station array antenna, dual-band antenna, multimode resonance, high selectivity.**

I. Introduction

With the growing demand for high-speed data transfer rates and increasing numbers of connected devices, 5G base station antennas (from sub-6 GHz to millimeter-wave frequencies) have become an essential component of modern communication systems. A 5G sub-6 GHz base station antenna is required to support the sub-6 GHz frequency bands that have been allocated for 5G wireless communication by regulatory bodies around the world. These lower frequency band antennas are important for 5G because they can provide better coverage and penetration through obstacles such as walls and buildings, as well as support for internet of things (IoT) devices.

The frequency bands n78 (3.3 GHz-3.8 GHz) and n79 (4.8 GHz-5.0 GHz) are crucial sub-6 GHz frequency bands for 5G communication and have been adopted by numerous countries worldwide. Recently, some innovative antennas were designed in [1]-[13] to cover part or single of these frequency bands. However, in nowadays integrated base station systems, single-band antennas are not sufficient for providing extensive frequency range coverage within the limited space. Thus, there is a growing interest in the research of dual/multi-band antennas. In addition to the dual/multi-band characteristics, filtering performance is also crucial for base station antennas to reduce the mutual coupling with other antennas. Therefore, the design of a dual-polarized antenna that possesses dual-frequency bands and filtering capability is of great significance for base station systems.

Traditionally, the filter and antenna were designed independently and then connected [14]. While this approach could yield a good filtering response, the resulting combination tended to be bulky, making it unsuitable for highly integrated communication systems that are prevalent today. In [15], by reshaping the final resonator of a traditional bandpass filter, a filtering antenna covering 2.26 GHz -2.66 GHz was realized. In this design, the final resonator acts not only as a resonator of the bandpass filter, but also the radiator of the antenna. By integrated two bandpass filters to an ultra-wideband antenna, a novel reconfigurable filtering antenna with three switchable states was presented in [16]. Similarly, by introducing filtering circuits on the feeding structures, some filtering antennas with good gain suppression levels were proposed in [17] and [18]. However, the bandwidths of these antennas are relativity narrow.

Apart from the methods mentioned above, filtering antenna usually be realized by introducing radiation nulls in unwanted

This work was supported in part by the Engineering and Physical Sciences Research Council (EPSRC) under Grant EP/S005625/1 and EP/N032497/1, in part by Huawei Technologies Ltd, in part by China Scholarship Council, and in part by Royal Society - International Exchanges 2019 Cost Share (NSFC) under Grant IEC\NSFC\191780. *(Corresponding author: Xuekang Liu.)*

Xuekang Liu and Benito Sanz-Izquierdo are with the School of Engineering, University of Kent, Canterbury CT2 7NT, U.K. (e-mail: xl255@kent.ac.uk).

Haiwei Zhang is with the Huawei Technologies Ltd, China.

Steven Gao is with the Dept of Electronic Engineering, Chinese University of Hong Kong.

Wei. Hu is with National Laboratory of Science and Technology on Antennas and Microwaves, Xidian University, Xi'an, Shaanxi 710071, China.

Xue-Xia Yang is with the School of Communication and Information Engineering, Shanghai University, Shanghai 200444, China.

Josaphat Tetuko Sri Sumantyo is with the Center for Environmental Remote Sensing, Chiba University, Chiba 263-8522, Japan.

This work is licensed under a Creative Commons Attribution 4.0 License. For more information, see https://creativecommons.org/licenses/by/4.0/

This article has been accepted for publication in IEEE Transactions on Antennas and Propagation. This is the author's version which has not been fully edited and content may change prior to final publication. Citation information: DOI 10.1109/TAP.2023.3322198

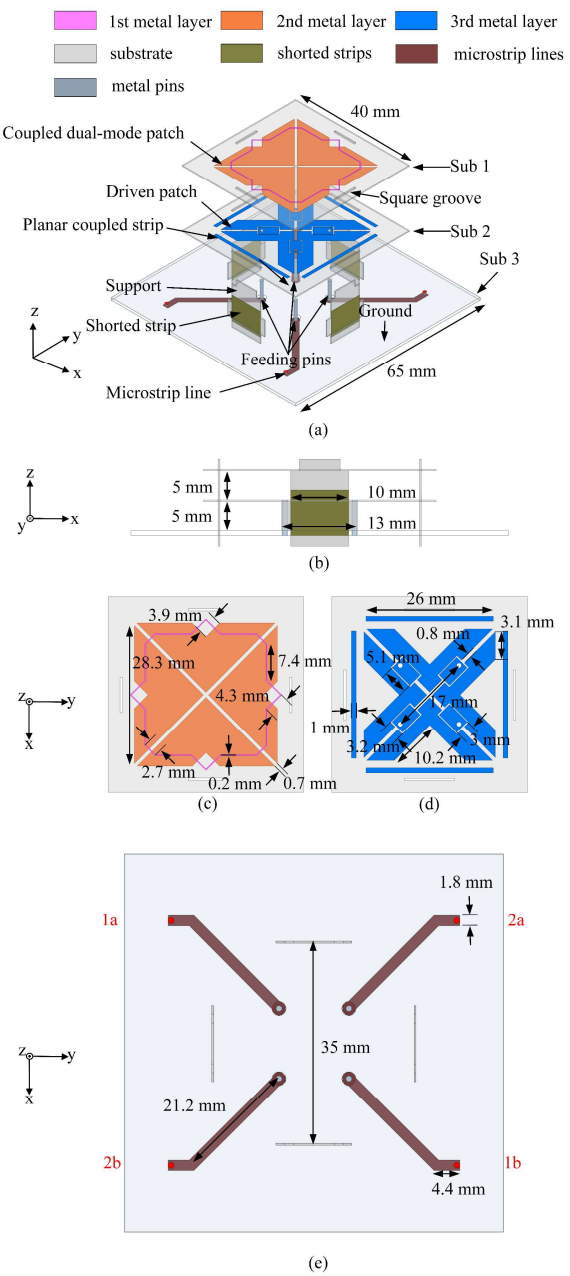

Fig. 1. Structure of the proposed design. (a) component breakdown view, (b) lateral view, (c) overhead view of top substrate, (d) overhead view of middle substrate, and (e) transmission line layer.

frequency bands to suppress the radiation [19]-[24]. By introducing parasitic loops above and below the dipole arms, a dual-polarized filtering antenna with two radiation nulls was achieved in [19]. This antenna can cover a wide frequency range from 1.66 GHz to 2.73 GHz with a stable gain. In [21], a dual-polarized filtering antenna covering 2.3 GHz- 2.9 GHz was realized by using defected ground structures (DGSs). However, the radiation patterns of this antenna are not stable within the working band. By exciting the out-of-band resonant mode of the feeding structure and radiator, a novel filtering antenna without additional filtering structure was presented in [23].

Some dual-band filtering antennas were achieved in [25]-[27] to work at the target 5G sub-6G frequency bands. However, all these antennas have single polarization. They are not suitable for base stations. In [28] and [29], two dual-band dual-polarized filtering antennas with band-notch characteristics were presented to cover the target frequency bands. The impedance bandwidths of them are 11.4% (lower band); 5.1% (higher band) and 19.8% (lower band); 13.2% (higher band). However, the out-of-band rejection level of these antennas are relatively low. By introducing filtering circuit on the feeding structure and etching slots on the radiator, a dual-band dual-polarized filtering antenna was achieved in [30]. This antenna has a good gain suppression level at out-of-bands. However, the impedance bandwidth of its lower band is relatively narrow to cover the 3.3 GHz -3.8 GHz band.

In this paper, by integrating a dual mode coupled patch, four planar coupled strips, and four shorted strips around the driven patch, four resonant modes and four radiation nulls can be successfully realized to cover the n78 (3.3 GHz-3.8 GHz) and n79 (4.8 GHz-5.0 GHz) bands. Different from other parasitic patches, the coupled patch in this design has two resonant modes within the frequency band from 2.5 GHz to 6.5 GHz. The additional resonant mode is obtained by simply etching a pair of crossing open slots on the patch. The resonant frequency of this mode can be modified by manually adjusting the parasitic loop located above the coupled patch. Four shorted strips are introduced to improve the out-of-band rejection level and half power beamwidth (HPBW) of the antenna. This results in the appearance of a 4th radiation null, and an improvement in the HPBW from 52° to 62°. To confirm the design concept, a four element array was also developed, produced, and evaluated. The experimental outcomes are consistent with the simulated data. The Ansys HFSS software was utilized to generate all simulated results.

II. Configuration of the Antenna Element

Fig. 1 provides a visual representation of the configuration for the proposed dual-band, dual-polarized filtering antenna element. The antenna is composed of a driven patch, four planar coupled strips, a coupled patch, a parasitic loop, and four shorted strips. All these structures are printed on Rogers 4003 substrates, as depicted in Fig. 1(a). The thickness of substrates 1 and 2 is 0.305 mm, while substrate 3 has a thickness of 0.813 mm. Fig. 1(b) shows the lateral view of the proposed antenna. The supports and super glue play a crucial role in ensuring the stability of each layer in this design. The supports serve two primary purposes. Firstly, they enable the realization of the shorting strip through PCB technology. Secondly, they maintain the proper spacing between the three substrates. By appropriately sizing the square grooves on the substrates, the supports securely clamp the substrates in place. Additionally, applying super glue at the junction of the square groove and the support eliminates the need for screws, providing a stable structure for the antenna. Fig. 1(c) and Fig .1(d) show the detailed dimensions for each component. By feeding the proposed two-layer radiator with four 50 Ω

This work is licensed under a Creative Commons Attribution 4.0 License. For more information, see https://creativecommons.org/licenses/by/4.0/

This article has been accepted for publication in IEEE Transactions on Antennas and Propagation. This is the author's version which has not been fully edited and content may change prior to final publication. Citation information: DOI 10.1109/TAP.2023.3322198

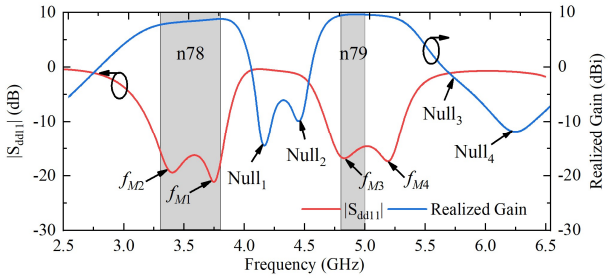

Fig. 2. Simulated $|S_{dd11}|$ and boresight realized gain of the antenna element.

microstrip lines, a dual-band dual-polarized antenna element with filter response is presented. The detailed design parameters of the microstrip lines are shown in Fig. 1(e). The S-parameters of the differential ports can be obtained by using the following equations:

$$S_{dd11} = (S_{1a1a} + S_{1b1b} - S_{1a1b} - S_{1b1a})/2 \quad (1)$$

$$S_{dd22} = (S_{2a2a} + S_{2b2b} - S_{2a2b} - S_{2b2a})/2 \quad (2)$$

$$S_{dd21} = (S_{2a1a} + S_{2b1b} - S_{2a1b} - S_{2b1a})/2 \quad (3)$$

$$S_{dd12} = (S_{1a2a} + S_{1b2b} - S_{1a2b} - S_{1b2a})/2 \quad (4)$$

The excitation of the multi resonant modes and the introduction of the radiation nulls will be interpreted in the section III.

III. Radiation Nulls and Multi-Resonance

The simulated reflection coefficient and boresight realized gain of the proposed antenna can be observed in Fig. 2. As depicted, the proposed antenna can cover the desired n78 (3.3-3.8 GHz) and n79 (4.8- 5.0 GHz) bands with four resonances The simulated gains within the operating bands can achieve 8.8 dBi and 9.6 dBi. Besides, this antenna has four radiation nulls within the frequency band 2.5 GHz to 6.5 GHz. Two of them are between the two target 5G Sub-6GHz bands. The other two are at higher out-of-band. The 1st, 2nd, and 3rd radiation nulls in this design are realized by introducing the coupled resonators, while the 4th radiation null is introduced by the shorted strips. To explain the working principles of the proposed antenna, coupled resonator filter topology will be introduced first.

Coupled resonator topology is a grouping of resonant circuits that are interconnected in a way that enables energy exchange and interaction. Multiple resonators are connected to one another in this topology via a common coupling element, like a capacitor or an inductor. The coupling component enables energy exchange and mutual behavior modification between the resonators. In coupled resonator topology, there are several paths from the source to the load. Transmission zeros can be obtained if the signals in the paths are equal in amplitude but opposite in phase [31]. Undoubtedly, this technique proves to be effective in introducing resonant modes and radiation nulls for the design of broadband/multiband

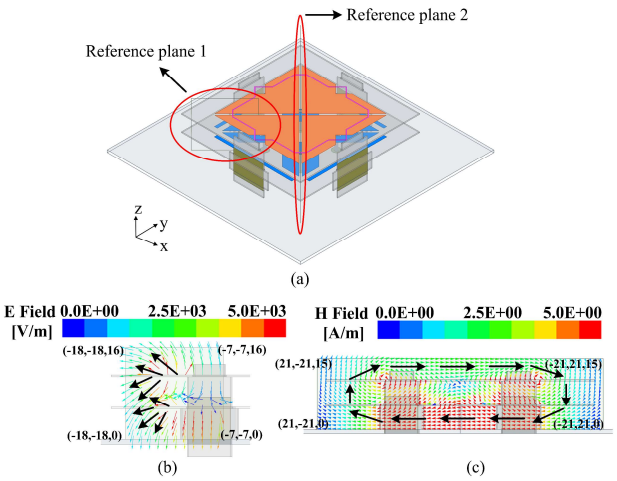

Fig. 3. (a) Configuration of the reference planes, (b) simulated E-field distribution on reference plane 1, and (c) simulated H-field distribution on reference plane 2 at f_{M2}.

filtering antennas. Nevertheless, the challenges lie in the introduction and allocation of the coupled resonators.

It can be observed from Fig. 2 that there are four resonant modes in this design. The 1st (M_1) resonant mode is the TM_{10} mode of the driven patch. The 2nd (M_2) and 4th (M_4) resonant modes are TM_{10} and open slot mode of the coupled dual-mode patch. The 3rd (M_3) resonant mode is the resonant mode of the planar coupled strip. All these resonant modes can be equivalent to parallel LC resonators. At their resonant frequencies, the phase of the transmission coefficient will be 0 and the RF signal will be transmitted to the free space. However, this shunt LC pair will show different properties at off-resonance frequencies. If the RF signal is above the resonant frequency, the resonator will provide a -90° phase shift. If the RF signal is below the resonant frequency, the phase shift will be +90°. It can be concluded as [31]:

$$\varphi \approx -90° \text{ (above)} \quad (5)$$

$$\varphi \approx +90° \text{ (below)} \quad (6)$$

Since all these coupled resonators (coupled structures) are coupled to the main resonator (driven patch), the coupling between the driven patch and the coupled structures are assumed as the main part when calculating the phase shift. The interference among coupled resonators will be ignored. Based on the above information, the radiation nulls of this antenna will be analyzed using multi-path topology.

A. 1st Radiation Null

The 1st radiation null in this design is caused by the coupled patch. Due to coupling between the driven patch and coupled patch, the TM_{10} mode (M_2) of the coupled patch can be excited. Thus, here are two paths from the input port to the output port around f_{M2}. They are P_i-M_1-M_2-P_o and P_i-M_1-P_o. Since both paths contain the same part P_i-M_1, it will not be included when calculating the phase difference between the main path and coupled path. Additionally, the path from the resonators to the

This work is licensed under a Creative Commons Attribution 4.0 License. For more information, see https://creativecommons.org/licenses/by/4.0/

This article has been accepted for publication in IEEE Transactions on Antennas and Propagation. This is the author's version which has not been fully edited and content may change prior to final publication. Citation information: DOI 10.1109/TAP.2023.3322198

TABLE I
PHASE SHIFT BETWEEN THE MAIN AND COUPLED PATHS

Path	Below f_{M2}	Above f_{M2}
P_i-M_1-P_o	0°	0°
P_i-M_1-M_2-P_o	-90°+90°	-90°-90°
	In phase	Out-of-phase

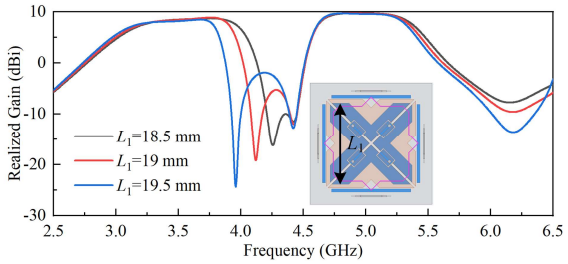

Fig. 4. Simulated boresight realized gain under different L_1.

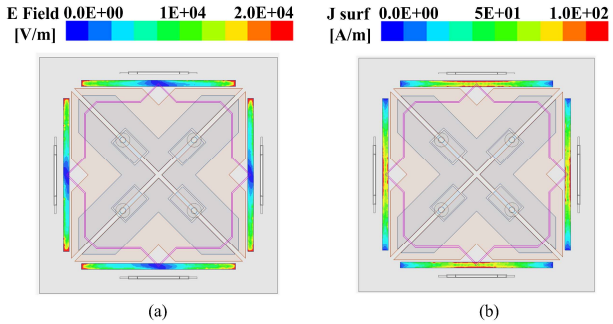

Fig. 5. Simulated (a) E field distribution, and (b) current distribution on the parasitic strips at 5.2 GHz.

output port will not contribute to the phase shift [4]. Thus, we only need to take the phase shift of the coupling and the phase shift provided by the coupled resonator into consideration.

The simulated electric and magnetic field distributions of the proposed antenna on the reference planes at f_{M2} are shown in Fig.3. Since the E-field vector does not extend from the driven patch to the coupled patch, there is no electric coupling between them. In contrast, the coupling between the driven patch and coupled patch can be classified as a magnetic coupling, as the H-field forms a closed loop.

The phase shift of the two dominate paths are given in Table I. Without loss of generality, the phase shift of the parasitic path (P_i-M_1-P_o) is assumed to be 0°. Due to the magnetic coupling between the driven patch and coupled patch, a -90° is introduced in the main path (P_i-M_1-M_2-P_o). Then, considering the phase shift that the 2nd resonant mode provided, a transmission zero will appear at the frequencies above f_{M2}. The simulated boresight realized gain of the proposed antenna under different L_1 is shown in Fig. 4. As can be observed, the 1st radiation null can be adjusted by changing the length of the L_1 with nearly no effect on other radiation nulls.

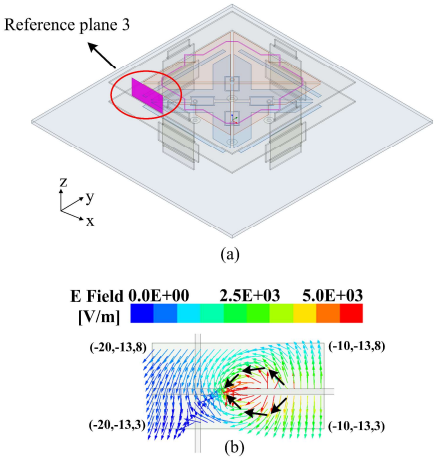

Fig. 6. (a) Configuration of the reference plane 3, (b) simulated E-field distribution on reference plane 3 at f_{M3}.

TABLE II
PHASE SHIFT BETWEEN THE MAIN AND COUPLED PATHS

Path	Below f_{M3}	Above f_{M3}
P_i-M_1-P_o	0°	0°
P_i-M_1-M_3-P_o	90°+90°	90°-90°
	Out-of-phase	In phase

B. 2nd Radiation Null

The 2nd radiation null in this design is obtained by the planar coupled strip. These coupled strips can be interpreted as resonators with a length of $\lambda_g/2$ (where λ_g represents the guided wavelength) [32]. Fig. 5 illustrates their electromagnetic characteristics, which resemble those of printed dipole antennas. When the parasitic strip resonates, the E-field reaches its maximum value at both ends of the strip. Conversely, there is an E-field null in the middle of the strip. However, the current distribution exhibits the opposite pattern, with the minimum current occurring at the strip's ends and the maximum current occurring at its center. The coupling between driven patch and the parasitic strip can excite a new resonant mode (M_3). Thus, a new path (P_i-M_1-M_3-P_o) for the RF signal can be achieved around f_{M3}. Since the phase shifts provided by the coupled resonator are fixed in the lower and upper frequency regions. the phase difference between the main path (P_i-M_1-M_3-P_o) and the parasitic path (P_i-M_1-P_o) is decided by the coupling method.

As mentioned above, when the parasitic strip resonates, the maximum E-field value appears at its two open ends. Therefore, electric coupling can be easily realized by placing one of the ends of the planar coupled strip close to the driven patch. The simulated E-field distribution on the reference plane 3 at f_{M3} is shown in Fig. 6. The electric coupling between the driven patch and planar coupled strip can be confirmed since the E-filed vector points from the driven patch to the parasitic strips. Fig. 7 shows the simulated boresight realized gain of the proposed antenna under different L_2. By increasing the length of the planar coupled strips, the

This work is licensed under a Creative Commons Attribution 4.0 License. For more information, see https://creativecommons.org/licenses/by/4.0/

This article has been accepted for publication in IEEE Transactions on Antennas and Propagation. This is the author's version which has not been fully edited and content may change prior to final publication. Citation information: DOI 10.1109/TAP.2023.3322198

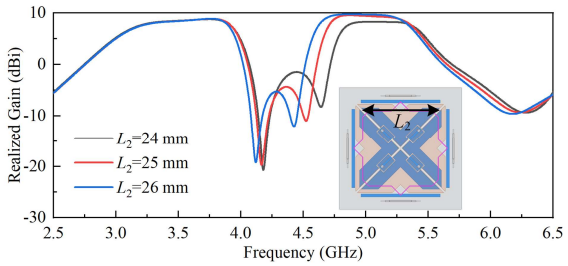

Fig. 7. Simulated boresight realized gain under different L_2.

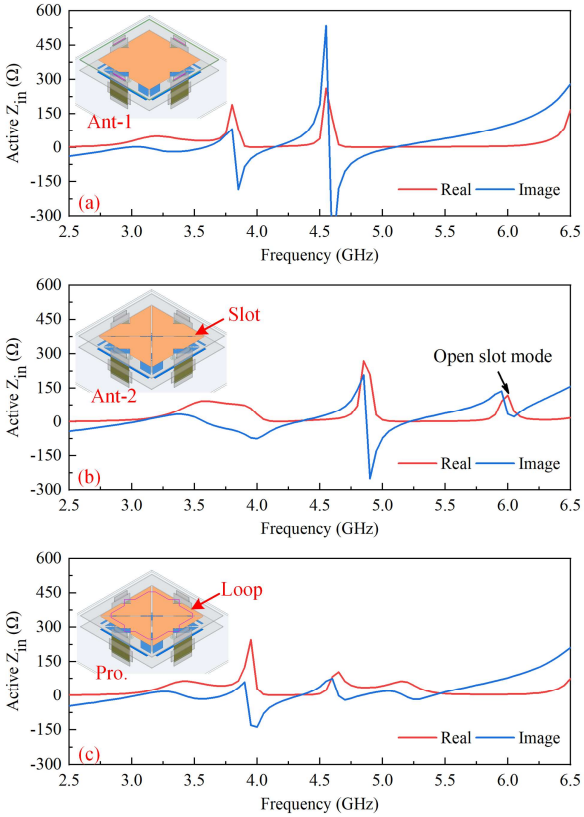

Fig. 8. Simulated input impedance of the (a) reference antenna 1, (b) reference antenna 2, and (c) the proposed antenna (without microstrip lines).

2nd radiation null can be easily shifted to lower frequency band with little influence on other radiation nulls.

C. 3rd Radiation Null and Open Slot Mode

The 3rd radiation null in this design is also introduced by the coupling between the driven patch and coupled patch. Different from traditional dual layer microstrip patch antenna, the coupled patch in this design has two resonant modes (TM_{10} mode and open slot mode). Thus, two radiation nulls can be introduced by this single coupled patch.

To explain the working principles of the coupled dual-mode patch more effectively, two reference antennas are designed and simulated. As shown in Fig.8, the open slots and parasitic polygon ring were removed in reference antenna 1 (Ant-1). While only the parasitic polygon ring was removed in reference antenna 2 (Ant-2). When the input impedance of the

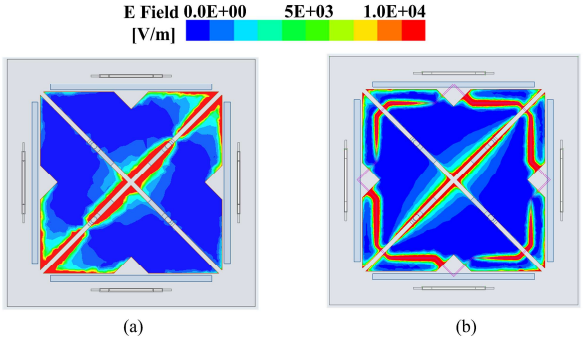

Fig. 9. Simulated E-field distributions on the coupled patch of the (a) reference antenna 2, and (b) proposed antenna.

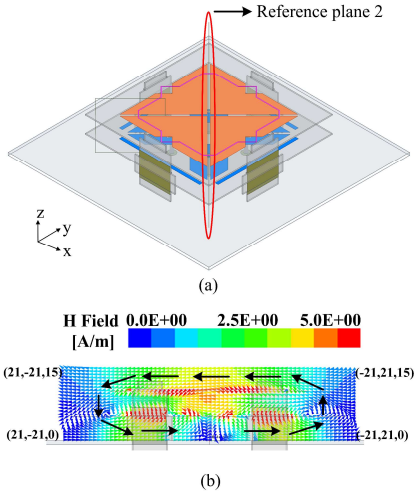

Fig. 10. (a) Configuration of the reference plane 2, (b) simulated H-field distribution on reference plane 2 at f_{M4}.

reference antennas in Fig. 8(a) and (b) is compared, it becomes apparent that the etched slots on the coupled patch have caused a new resonant mode to be excited at approximately 6 GHz. The simulated E-field distribution of the coupled patch of reference antenna 2 is shown in Fig. 9(a). As can be seen, the E-field density concentrate at the center part of the coupled patch. And there are two E-field nulls along the slots.

The introduction of the resonant mode at 6 GHz did not lead to a wide impedance bandwidth due to a significant frequency ratio (FR) between the strip mode and the new mode. To address this issue, a parasitic loop was added above the slot-loaded coupled patch to reduce the FR. The impact of the polygon loop is illustrated in Fig. 8(c), showing a shift in the resonant frequency of the open slot mode from 6 GHz to 5.2 GHz. Furthermore, Fig. 9(b) indicates that the antiphase point of the electric field moved towards the edges, resulting in a resonant frequency shift towards a lower frequency.

Since the maximum E-field of the driven patch is at its both ends, and the slot is in the center part. The coupling between the driven patch and the slots is magnetic coupling. This can be confirmed by the simulated H-field distribution on reference plane 2 in Fig. 10. Then, the phase shift of the main path around f_{M4} can be calculated. Table III indicates that the

This work is licensed under a Creative Commons Attribution 4.0 License. For more information, see https://creativecommons.org/licenses/by/4.0/

This article has been accepted for publication in IEEE Transactions on Antennas and Propagation. This is the author's version which has not been fully edited and content may change prior to final publication. Citation information: DOI 10.1109/TAP.2023.3322198

TABLE III
PHASE SHIFT BETWEEN THE MAIN AND COUPLED PATHS

Path	Below f_{M4}	Above f_{M4}
P_i-M_1-P_o	0°	0°
P_i-M_1-M_4-P_o	-90°+90°	-90°-90°
	In phase	Out-of-phase

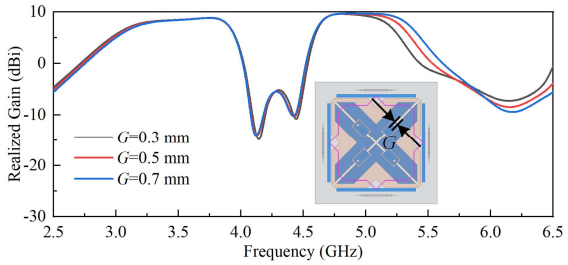

Fig. 11. Simulated boresight realized gain under different *G*.

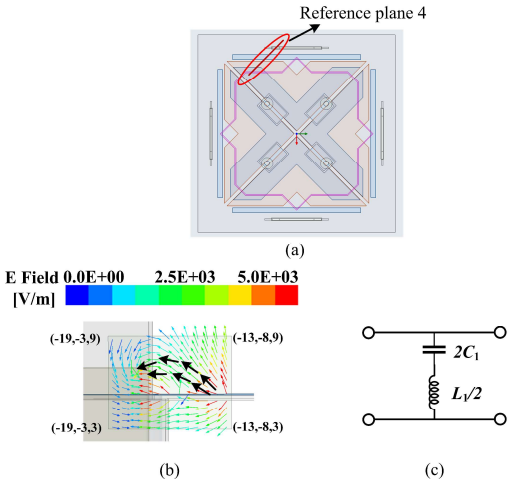

Fig. 12. (a) Configuration of the reference plane 4, (b) simulated E-field distribution on reference plane 4, and (c) equivalent circuit of the shorted strip.

main and secondary paths are in phase below f_{M4} but become out-of-phase above f_{M4}. This indicates the presence of a transmission zero above f_{M4}. The boresight realized gain of the proposed antenna with varying gap sizes (G) is shown in Fig. 11. As the gap size increases, the 3rd radiation null shifts towards a higher frequency band while the other radiation nulls remain unaffected.

D. 4th Radiation Null and Enhancement of HPBW

The 4th radiation null in this design is introduced by the shorted strips. However, different from other radiation nulls, this radiation null is not caused by the coupled resonator. The shorted strip can be equivalent to an inductor with one end connected to the ground. As shown in Fig.12, the open end of the shorted strip exhibit the highest electric field intensity and are in close proximity to the open ends of the driven patch where the maximum electric field also occurs. Thus, there will be electric coupling between the driven patch and shorted strips. The equivalent circuit of the shorted strip is shown in

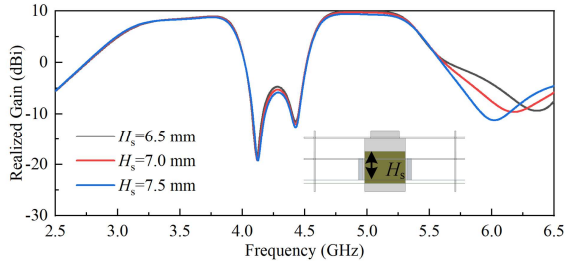

Fig. 13. Simulated boresight realized gain under different *Hs*.

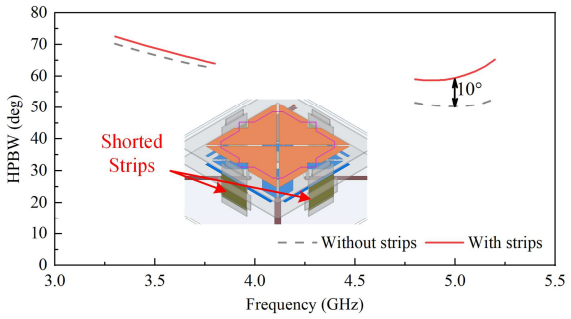

Fig. 14. Simulated HPBW of the proposed antenna with/without shorted strips.

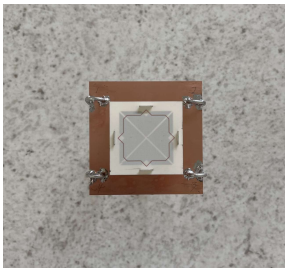

Fig. 15. Photo of the fabricated antenna element.

Fig. 12(c). At resonance, the series *LC* circuit acts as a short circuit, causing all power to be reflected to the source. Thus, a radiation null can be obtained. Fig. 13 displays the relationship between the height of the strip (H_s) and the frequency of the 4th radiation null. As can be seen, when H_s increases, the 4th radiation null shifts towards lower frequency band without influencing other radiation nulls.

Apart from filtering performance and impedance bandwidth, the half-power beamwidth (HPBW) plays a crucial role in evaluating the performance of a dual-band, dual-polarized filtering base station antenna. This parameter is closely associated with the coverage of the base station antenna. The incorporation of these shorted strips has a dual benefit of not only introducing a radiation null but also significantly enhancing the HPBW of the proposed antenna. Specifically, Fig. 14 demonstrates that the HPBW at higher band can be effectively increased to approximately 62° while having minimal impact on the HPBW at the lower band.

E. Results and Comparison

Fig. 15 shows the fabricated prototype of the proposed antenna. The performance of this fabricated antenna element was evaluated through S-parameter and far-field

This work is licensed under a Creative Commons Attribution 4.0 License. For more information, see https://creativecommons.org/licenses/by/4.0/

This article has been accepted for publication in IEEE Transactions on Antennas and Propagation. This is the author's version which has not been fully edited and content may change prior to final publication. Citation information: DOI 10.1109/TAP.2023.3322198

TABLE IV
COMPARISON OF THE PREVIOUSLY PRESENTED DUAL-BAND ANTENNAS

Ref.	Polar.	Operation Bands	Size (λ_L^3)	Method	Extra Circuit	Iso. (dB)	Gain (dBi)	HPBW	NNBOB	NN
[25]	Single	3.21-3.66 GHz (13.1%) 4.75-5.40 GHz (12.8%) $\|S_{11}\|$< -10 dB	0.77×0.77×0.06 (@3.21 GHz)	Stacked patch and u-slot	No	/	9.1;8.7	/	2	2
[27]	Single	3.23-3.85 GHz (17.5%) 5.29-5.74 GHz (8.2%) $\|S_{11}\|$< -10 dB	0.42×0.28×0.06 (@3.23 GHz)	Defected ground structure and differential feedlines	Yes	/	8.4; 9.5	/	2	5
[28]	Dual	3.28-3.7 GHz (11.4%) 4.75-5 GHz (5.1%) VSWR< 2	0.41×0.41×0.08 (@3.28 GHz)	Closed loop structure	No	40	8.3; 10.5	~90°* ~86°*	1	1
[29]	Dual	3.14-3.83 GHz (19.8%) 4.40-5.02 GHz (13.2%) $\|S_{11}\|$< -10 dB	0.37×0.37×0.12 (@3.14 GHz)	/	/	20	7.1; 8.2	/	/	/
[30]	Dual	3.28-3.71 GHz (12.3%) 4.8-5.18 GHz (7.6%) VSWR< 1.5	0.42×0.42×0.11 (@3.28 GHz)	Extra circuit on feeding lines and slots	Yes	37	8.7; 9.8	65° ± 4° 52° ± 5°	1	3
This Work	**Dual**	**3.24-3.83 GHz (16.7%) 4.74-5.30 GHz (11.2%) $\|S_{dd11}\|$< -14 dB**	**0.38×0.38×0.11** (@3.24 GHz)	**Coupled resonators and shorted strips**	**No**	**40**	**8.1; 8.8**	**68° ± 4° 62° ± 3°**	**2**	**4**

λ_L is the wavelength at the lowest operating frequency in free space. Polar. represents polarization. NNBOB represents Number of Nulls Between Operation Bands. Iso. represents isolation. NN represents number of nulls. The HPBWs with* mean they are HPBWs in E-plane and H-plane, rather than the HPBWs in horizontal plane.

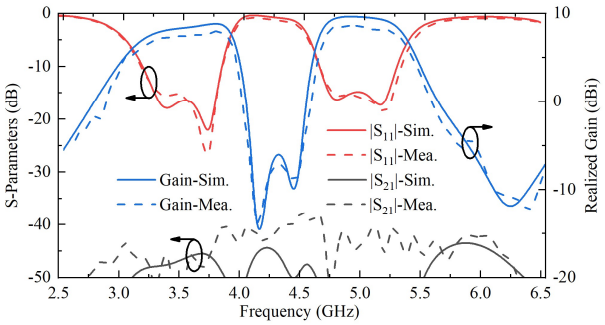

Fig. 16. Measured and simulated S-parameters and boresight realized gain of the proposed antenna element.

measurements conducted in the antenna lab at the University of Kent, using the Keysight P9377B Vector Network Analyzer and anechoic chamber. Fig. 16 illustrates the comparison between the measured and simulated S-parameters, revealing a close agreement between the two sets of results. From the measured results, it can be observed that the fabricated antenna operates effectively in two distinct frequency bands, spanning 3.24-3.83 GHz and 4.74-5.30 GHz, respectively. The two input ports of the antenna are well isolated with a measured isolation value of higher than 40 dB within the operating frequency bands. The proposed antenna achieves a maximum realized gain of 8.1 dBi and 8.8 dBi in the lower band and higher band, respectively. Furthermore, the realized gain outside of the two desired frequency bands can be effectively suppressed through the four radiation nulls.

The radiation patterns of the fabricated antenna in the horizontal plane at various frequencies are displayed in Fig. 17, revealing stable radiation patterns within the operating frequency bands. The measured HPBW of the antenna is around 68° (± 4°) in the lower band and approximately 62° (± 3°) in the higher band. The cross-polarization levels of the measured antenna are found to be less than -17 dB over a range of ±90° and less than -34 dB at the boresight direction.

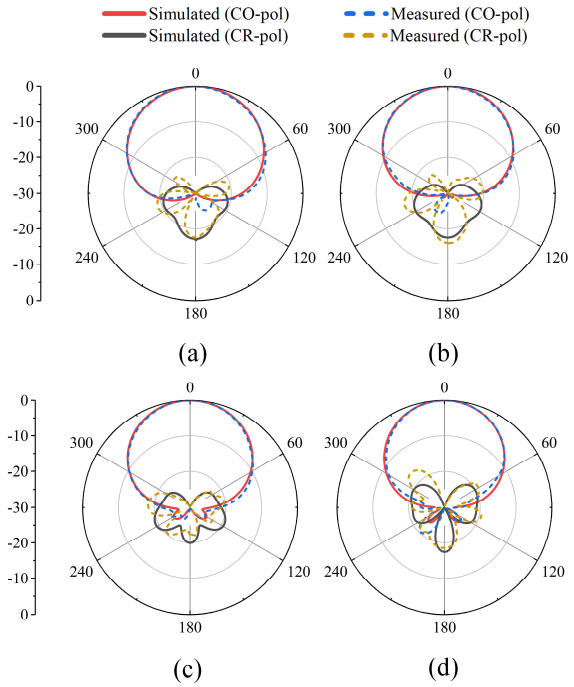

Fig. 17. Measured and simulated normalized radiation patterns of the proposed antenna element at (a) 3.3 GHz, (b) 3.6 GHz, (c) 3.8 GHz, and (d) 5.0 GHz.

Table IV provides a comparison of the key factors of the proposed antenna with those of previously published reference antennas. The antennas in [25] and [27] can cover two separate frequency bands with good out-of-band rejection level. However, both of these antennas are single polarized antenna which are not suitable for base station applications in 5G/6G. Since a dual-polarized antenna is not a simple combination of two single polarized antenna with two orthogonal polarization ports. The design of a dual-polarized antenna is more difficult than the design of a single polarized one. The antenna in [28] realizes a higher gain than the

This work is licensed under a Creative Commons Attribution 4.0 License. For more information, see https://creativecommons.org/licenses/by/4.0/

This article has been accepted for publication in IEEE Transactions on Antennas and Propagation. This is the author's version which has not been fully edited and content may change prior to final publication. Citation information: DOI 10.1109/TAP.2023.3322198

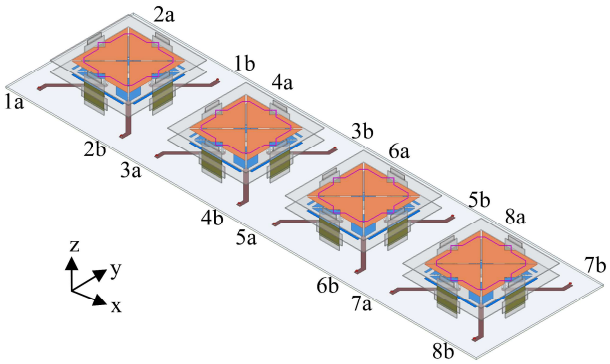

Fig. 18. Configuration of the proposed array antenna.

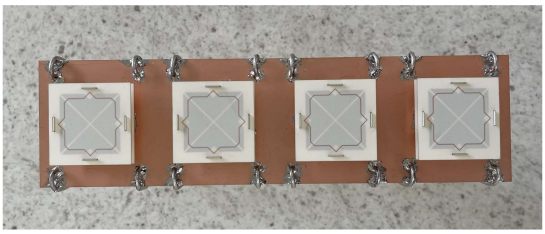

(a)

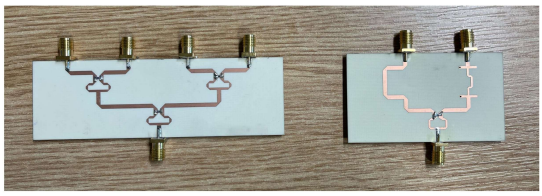

(b)

Fig. 19. Photo of (a) the fabricated array antenna, and (b) power divider and printed baluns.

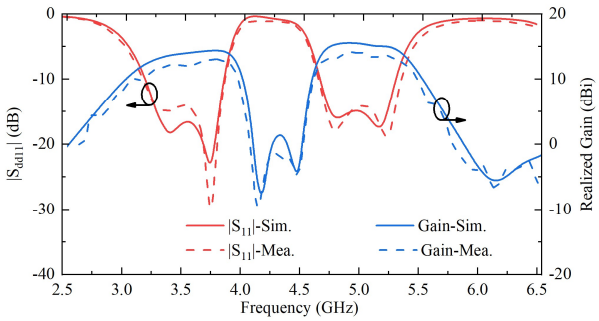

Fig. 20. Measured and simulated $|S_{dd11}|$ and boresight realized gain of the proposed array antenna.

proposed antenna with a larger radiator size. However, the impedance bandwidths of this antenna are 11.4% and 5.1% with a reference level of VSWR< 2 (It should be $|S_{11}|$< -14 dB in base station applications). It is worth noting that this design can not fully cover the target 5G sub-6GHz bands (3.3 GHz-3.8 GHz and 4.8 GHz- 5.0 GHz). Besides, our design obtains three additional radiating nulls compared to this antenna, which only exhibits a single radiating null. The design in [29] obtains a smaller radiator size than the proposed antenna, However, the isolation between the input ports is only 20 dB.

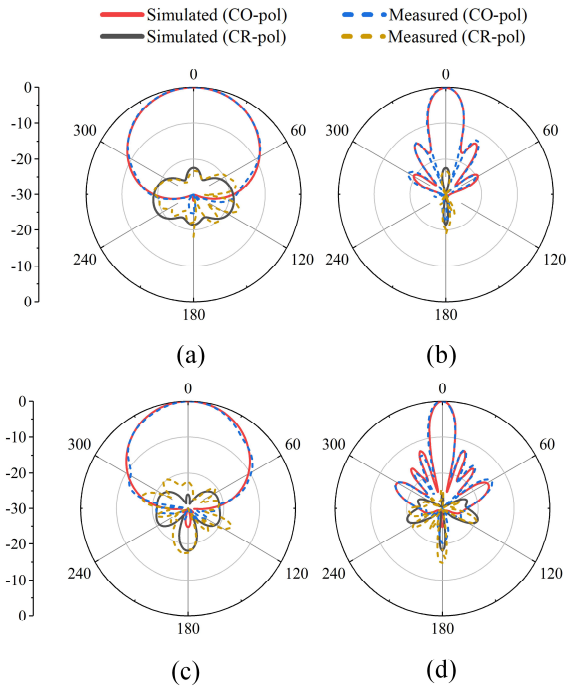

Fig. 21. Measured and simulated normalized radiation patterns of the proposed array antenna at (a) 3.6 GHz in horizontal plane, (b) 3.6 GHz in vertical plane, (c) 5.0 GHz in horizontal plane, and (d) 5.0 GHz in vertical plane.

When compared with the design presented in [30], our antenna exhibits a 35.7% wider impedance bandwidth in the lower band and a 47.4% wider impedance bandwidth in the higher band. The aperture of our antenna is only 81.8% of the size of the design in [30]. Moreover, the higher band HPBW of the antenna in reference [30] is only 52°, which is significantly narrower than that of the proposed antenna. Its narrow HPBW in the higher band limits its practical use in base station systems. Furthermore, the proposed design has more independently adjustable radiation nulls than the antenna in [30] without introducing extra circuit.

After a thorough comparison with other designs in the table, it can be concluded that the proposed antenna has superior overall performance and exhibits significant potential for employment in 5G base stations.

IV. Array Antenna

As shown in Fig. 18, by arranging four proposed antenna elements in a row, a 1×4 linear array antenna is realized. The spacing between these antenna elements is 60 mm. The entire array antenna's footprint is 240 mm × 65 mm. As depicted in Fig. 19, a prototype of the proposed array antenna was fabricated for the purpose of confirming the design concept.

The measured results in Fig. 20 shows that the proposed array antenna can cover two wide frequency ranges of 3.26 GHz -3.82 GHz and 4.72 GHz -5.31 GHz with a reference reflection coefficient level of -14 dB. Within these operation bands, the proposed array antenna realizes a peak gain of 13.2 dBi and 14.6 dBi. The variation between the measured gains and simulated gains is primarily attributed to measurement

This work is licensed under a Creative Commons Attribution 4.0 License. For more information, see https://creativecommons.org/licenses/by/4.0/

This article has been accepted for publication in IEEE Transactions on Antennas and Propagation. This is the author's version which has not been fully edited and content may change prior to final publication. Citation information: DOI 10.1109/TAP.2023.3322198

error and additional insertion loss introduced by the feeding network, coaxial cables, and SMA connectors. Besides, the radiation outside the two operation bands is successfully suppressed by the radiation nulls.

The normalized radiation patterns of the proposed array antenna were also tested and compared with the simulated results. The two planes of most interest for ±45° dual-polarized base station antennas are the horizontal plane and vertical plane, hence only these two planes were selected during the test. The measured radiation patterns of the fabricated array antenna agree well with the simulated results. However, there are some minor differences in the cross-polarization level, which could be caused by radiation from the cables and connectors. At the center frequency of the lower band, the proposed antenna exhibits a HPBW of 69° in the horizontal plane and 18° in the vertical plane, as depicted in Fig. 21(a) and (b). Figure 21(c) and (d) illustrate that the proposed antenna has a horizontal plane HPBW of 62° and a vertical plane HPBW of 12° at the center frequency of the higher band.

V. Conclusion

The main emphasis of this paper is the development of a dual-band, dual-polarized filtering antenna utilizing coupled structures. The integration of a dual mode coupled patch and four planar coupled strips surrounding the driven patch enables the attainment of four resonant modes and three radiation nulls. Further enhancement of the antenna's out-of-band rejection level and HPBW is achieved by introducing four shorted strips. As a result, a 4th radiation null is observed, and the HPBW is improved from 52° to 62°. The measured results for both the antenna element and its array were found to be consistent with the simulated results, indicating the accuracy of the design. Results from the testing also revealed that the proposed designs can effectively cover the targeted 5G spectrum for numerous countries. With its dual-wideband, dual-polarized filtering capabilities, this antenna is a promising candidate for use in 5G base-station applications.

References

[1] D. Yang, H. Zhai, C. Guo and C. Ma, "A novel differentially fed dual-polarized filtering magneto-electric dipole antenna for 5G base station applications," *IEEE Trans. Antennas Propag*., vol. 70, no. 7, pp. 5373-5382, July 2022.

[2] A. Alieldin, Y. Huang, M. Stanley, S. D. Joseph and D. Lei, "A 5G MIMO antenna for broadcast and traffic communication topologies based on pseudo inverse synthesis," *IEEE Access*, vol. 6, pp. 65935-65944, 2018.

[3] K. Xue, D. Yang, C. Guo, H. Zhai, H. Li, and Y. Zeng, "A dual-polarized filtering base-station antenna with compact size for 5G applications," *IEEE Antennas Wireless Propag. Lett.*, vol. 19, no. 8, pp. 1316-1320, Aug. 2020.

[4] J. -F. Qian, F. -C. Chen, Q. -X. Chu, Q. Xue and M. J. Lancaster, "A novel electric and magnetic gap-coupled broadband patch antenna with improved selectivity and its application in MIMO system," *IEEE Trans. Antennas Propag*., vol. 66, no. 10, pp. 5625-5629, Oct. 2018.

[5] Y. Luo, J. Lai, N. Yan, W. An, and K. Ma, "Codesign of single-layer dual-polarized dual compressed high-order modes differentially fed patch antenna and solar cells for green communication," *IEEE Trans. Antennas Propag*., vol. 70, no. 3, pp. 2289-2294, March 2022.

[6] L. -H. Wen, S. Gao, Q. Luo, Q. Yang, W. Hu, and Y. Yin, "A low-cost differentially driven dual-polarized patch antenna by using open-loop resonators," *IEEE Trans. Antennas Propag*., vol. 67, no. 4, pp. 2745-2750, April 2019.

[7] C. Hua, R. Li, Y. Wang and Y. Lu, "Dual-polarized filtering antenna with printed jerusalem-cross radiator," *IEEE Access*, vol. 6, pp. 9000-9005, 2018.

[8] Y. Li, Z. Zhao, Z. Tang and Y. Yin, "Differentially-fed, wideband dual-polarized filtering antenna with novel feeding structure for 5G Sub-6 GHz base station applications," *IEEE Access*, vol. 7, pp. 184718-184725, 2019.

[9] Y. Zhang, Y. Zhang, D. Li, Z. Niu and Y. Fan, "Dual-polarized low-profile filtering patch antenna without extra circuit," *IEEE Access*, vol. 7, pp. 106011-106018, 2019.

[10] W. Chen, Z. Yu, X. He, J. Zhou and W. Hong, "Enhanced-stopband dual-polarized filtenna without extra circuit for tile array applications," *IEEE Trans. Antennas Propag*., vol. 70, no. 8, pp. 7193-7198, Aug. 2022.

[11] X. Liu et al., "A mutual-coupling-suppressed dual-band dual-polarized base station antenna using multiple folded-dipole antenna," *IEEE Trans. Antennas Propag*., vol. 70, no. 12, pp. 11582-11594, Dec. 2022.

[12] H. Yuan, F. -C. Chen and Q. -X. Chu, "A wideband and high gain dual-polarized filtering antenna based on multiple patches," IEEE Trans. Antennas Propag., vol. 70, no. 10, pp. 9843-9848, Oct. 2022.

[13] M. Ciydem and E. A. Miran, "Dual-polarization wideband sub-6 GHz suspended patch antenna for 5G base station," *IEEE Antennas Wireless Propag. Lett.*, vol. 19, no. 7, pp. 1142-1146, July 2020.

[14] G. Goussetis and D. Budimir, "Antenna filter for modern wireless systems," *Proc. 32nd Eur. Microw. Conf.*, 2002, pp. 1–3.

[15] W. -J. Wu, Y. -Z. Yin, S. -L. Zuo, Z. -Y. Zhang and J. -J. Xie, "A new compact filter-antenna for modern wireless communication systems," *IEEE Antennas Wireless Propag. Lett.*, vol. 10, pp. 1131-1134, 2011.

[16] J. Deng, S. Hou, L. Zhao and L. Guo, "A reconfigurable filtering antenna with integrated bandpass filters for UWB/WLAN applications," *IEEE Trans. Antennas Propag*., vol. 66, no. 1, pp. 401-404, Jan. 2018.

[17] K. -R. Xiang, F. -C. Chen, Q. Tan and Q. -X. Chu, "Design of novel printed filtering dipole antennas," *IEEE Trans. Antennas Propag*., vol. 69, no. 5, pp. 2537-2545, May 2021.

[18] K. -R. Xiang, F. -C. Chen, Q. Tan and Q. -X. Chu, "High-selectivity filtering patch antennas based on multipath coupling structures," *IEEE Trans. Microw. Theory Techn.*, vol. 69, no. 4, pp. 2201-2210, April 2021.

[19] C. F. Ding, X. Y. Zhang, Y. Zhang, Y. M. Pan and Q. Xue, "Compact broadband dual-polarized filtering dipole antenna with high selectivity for base-station applications," *IEEE Trans. Antennas Propag*., vol. 66, no. 11, pp. 5747-5756, Nov. 2018.

[20] Z. Zheng, D. Li, X. Tan and Q. Chen, "A compact low-profile differential dual-polarized filtenna without an external filter circuit for vehicular communications," *IEEE Transactions on Vehicular Technology*., doi: 10.1109/TVT.2022.3230220.

[21] W. Yang, M. Xun, W. Che, W. Feng, Y. Zhang and Q. Xue, "Novel compact high-gain differential-fed dual-polarized filtering patch antenna," *IEEE Trans. Antennas Propag*., vol. 67, no. 12, pp. 7261-7271, Dec. 2019.

[22] X. Liu et al., "A compact dual-polarized filtering antenna with steep cut-off for base-station applications," *IEEE Trans. Antennas Propag*., vol. 70, no. 7, pp. 5941-5946, July 2022.

[23] Y. F. Cao, Y. F. Wu, Y. -M. Pan and X. Y. Zhang, "A method of generating radiation nulls utilizing inherent resonance modes for dual-polarized filtering dipole antenna design," *IEEE Trans. Antennas Propag*., vol. 68, no. 8, pp. 6413-6418, Aug. 2020.

[24] C. -X. Mao, S. Gao, Y. Wang, Q. Luo, and Q. -X. Chu, "A shared-aperture dual-band dual-polarized filtering-antenna-array with improved frequency response," *IEEE Trans. Antennas Propag*., vol. 65, no. 4, pp. 1836-1844, April 2017.

[25] J. Hao, N. Yan, Y. Luo, H. Fu and K. Ma, "A low-cost dual-band multimode high-gain stacked-patch antenna based on SISL for 5G applications," *IEEE Antennas Wireless Propag. Lett.*, vol. 21, no. 1, pp. 4-8, Jan. 2022.

[26] Y. -M. Zhang and S. Zhang, "Two-port dual-band filtering network and its application on filtering antennas," *IEEE Antennas Wireless Propag. Lett.*, vol. 22, no. 4, pp. 679-683, April 2023.

[27] D. Li, M. -C. Tang, Y. Wang, K. -Z. Hu, and R. W. Ziolkowski, "Dual-band, differentially-fed filtenna with wide bandwidth, high selectivity,

This work is licensed under a Creative Commons Attribution 4.0 License. For more information, see https://creativecommons.org/licenses/by/4.0/

This article has been accepted for publication in IEEE Transactions on Antennas and Propagation. This is the author's version which has not been fully edited and content may change prior to final publication. Citation information: DOI 10.1109/TAP.2023.3322198

and low cross-polarization," *IEEE Trans. Antennas Propag.*, vol. 70, no. 6, pp. 4872-4877, June 2022.
[28] B. Feng, L. Li, J. -C. Cheng, and C. -Y. -D. Sim, "A dual-band dual-polarized stacked microstrip antenna with high-isolation and band-notch characteristics for 5G microcell communications," *IEEE Trans. Antennas Propag.*, vol. 67, no. 7, pp. 4506-4516, July 2019.
[29] Q. Liu, H. Liu, W. He and S. He, "A low-profile dual-band dual-polarized antenna with an AMC reflector for 5G communications," *IEEE Access*, vol. 8, pp. 24072-24080, 2020.
[30] Y. Li, Z. Zhao, Z. Tang, and Y. Yin, "Differentially fed, dual-band dual-polarized filtering antenna with high selectivity for 5G Sub-6 GHz base station applications," *IEEE Trans. Antennas Propag.*, vol. 68, no. 4, pp. 3231-3236, April 2020.
[31] J. B. Thomas, "Cross-coupling in coaxial cavity filters - a tutorial overview," *IEEE Trans. Microw. Theory Techn.*, vol. 51, no. 4, pp. 1368-1376, April 2003.
[32] J.-S. G. Hong and M. J. Lancaster, *Microstrip Filters for RF/Microwave Applications.* New York, NY, USA: Wiley, 2001.

Xuekang Liu (Graduate Student Member, IEEE) received the M.S. degree (Hons.) in the electromagnetic field and microwave technology from Xidian University, Xi'an, China, in 2020. He is currently pursuing the Ph.D. degree with the School of Engineering, University of Kent, Canterbury, U.K. His current research interests include multiband base station antennas, filtering antennas, microstrip antennas, circularly polarized antennas, terminal antennas, and omnidirectional antennas.,Mr. Liu was a recipient of the Best Student Paper Award from the 17th International Workshop on Antenna Technology (iWAT 2022), Dublin, and the Outstanding Academic Achievement for his M.S. program. He received the Young Scientist Award from the International Union of Radio Science (URSI) Member Committee, Germany, 2022.

Benito Sanz-Izquierdo received the B.Sc. degree from the Universidad de Las Palmas de Gran Canaria (ULPGC), Las Palmas de Gran Canaria, Spain, and the M.Sc. and Ph.D. degrees from the University of Kent, Canterbury, U.K., in 2007.

In 2012, he worked with Harada Industries Ltd., Birmingham, U.K., where he developed novel antennas for the automotive industry. He was a Research Associate with the School of Engineering, University of Kent, in 2013, where he became a Lecturer in electronic systems and a Senior Lecturer in 2018. His research has been funded by a variety of sources, such as the U.K. Engineering and Physical Sciences Research Council (EPSRC), the Royal Academy of Engineering, and the Royal Society. His research interests include multiband antennas, wearable electronics, additive manufacturing (3-D printing), substrate integrated waveguides components, metamaterials, electromagnetic band-gap structures, frequency selective surfaces, and reconfigurable devices.

Dr. Sanz-Izquierdo has received awards and recognitions for his work on wearable antennas (mention in the House of Lords and the IEEE International Workshop on Antenna Technology (IWAT) Best Paper Award), frequency selective surfaces (the Best Paper at the Institution of Engineering and Technology (IET) Workshop on Aerospace Applications Award), and reconfigurable antennas (the 2017 CST University Publication Award for an IEEE TRANSACTIONS article), among others.

Haiwei Zhang received the B.S. and M.S. degrees in electronics engineering from Xidian University in 2009 and 2012, respectively, and the Ph.D. degree in electronics engineering from the City University of Hong Kong in 2016.

He joined Huawei Technologies Company, Ltd., in 2016, where he was involved with the development of various antennas and RF components/sub-systems for the 5G and beyond wireless communications.

Dr. Zhang was awarded the Hong Kong Ph.D. Fellowship in 2012.

Steven Gao (Fellow, IEEE) received the PhD from Shanghai University, China, in 1999.

He is currently a Professor with the Department of Electronic Engineering, Chinese University of Hong Kong. Prior to this, he was a Chair Professor with the University of Kent, UK for nearly 10 years. He has co-authored/co-edited three books, such as Space Antenna Handbook (Wiley, 2012), Circularly Polarized Antennas (IEEE & Wiley, 2014), and Low-Cost Smart Antennas (Wiley, 2019); over 400 articles; and 20 patents. His research covers smart antennas, phased arrays, MIMO, reconfigurable antennas, broadband/multiband antennas, satellite antennas, RF/microwave/mm-wave/THz circuits, mobile communications, satellite communications, UWB radars, synthetic aperture radars (SARs), sensors, the Internet of Things (IoT), and small satellites.

Dr. Gao is a fellow of the Royal Aeronautical Society and Institution of Engineering and Technology (IET). He served as the General Chair for international conferences, such as Loughborough Antennas and Propagation Conference (LAPC) in 2013 and UK, Europe, China Millimeter Waves and THz Technology Workshop (UCMMT) in 2021 and was an invited/keynote speaker at many conferences. He also serves as an Associate Editor for several international journals, such as IEEE TRANSACTIONS ON ANTENNAS AND PROPAGATION, Radio Science, Electronics Letters, and IET Circuits, Devices and Systems; and the Editor-in-Chief for Book Series on Microwave and Wireless Technologies (John Wiley & Sons). He is the Lead Guest Editor of IEEE TRANSACTIONS ON ANTENNAS AND PROPAGATION for a Special Issue on Low-Cost Wide-Angle Beam-Scanning Antennas in 2022. He served as the Lead Guest Editor for PROCEEDINGS OF THE IEEE for a Special Issue on Small Satellites in 2018 and IEEE TRANSACTIONS ON ANTENNAS AND PROPAGATION for a Special Issue on Antennas for Satellite Communication in 2015, and a Guest

This work is licensed under a Creative Commons Attribution 4.0 License. For more information, see https://creativecommons.org/licenses/by/4.0/

This article has been accepted for publication in IEEE Transactions on Antennas and Propagation. This is the author's version which has not been fully edited and content may change prior to final publication. Citation information: DOI 10.1109/TAP.2023.3322198

Editor for IET Circuits, Devices, and Systems for a Special Issue on Photonic and RF Communications Systems in 2014. He is the U.K.'s Representative at the European Association on Antennas and Propagation (EurAAP). He was a Distinguished Lecturer of the IEEE Antennas and Propagation Society.

Wei Hu (Senior Member, IEEE) received the Ph.D. degree in electromagnetic fields and microwave technology from Xidian University, Xi'an, China, in 2013.

From 2018 to 2019, he was an Academic Visitor with the University of Kent, Canterbury, U.K. He is currently a Full Professor with the National Key Laboratory of Antennas and Microwave Technology, Xidian University. He has authored or co-authored more than 100 internationally refereed journal articles. His current research interests include multiband and wideband antennas, circularly polarized antennas, MIMO antenna arrays, and wideband wide-scanning phased arrays.

Xue-Xia Yang (Senior Member, IEEE) received the B.S. and M.S. degrees from Lanzhou University, Lanzhou, China, in 1991 and 1994, respectively, and the Ph.D. degree in electromagnetic field and microwave technology from Shanghai University, Shanghai, China, in 2001. From 1994 to 1998, she was a Teaching Assistant and a Lecturer with Lanzhou University. From 2001 to 2008, she was a Lecturer and an Associate Professor with Shanghai University. She is currently a Professor and the Head of the Antennas and Microwave Research and Development Center, Shanghai University. She has authored or coauthored over 180 technical journal and conference papers. Her research interests include antennas theory and technology, computational electromagnetics, and microwave power transmission. Dr. Yang is a member of the Committee of Antenna Society of China Electronics Institute and a Senior Member of China Electronics Institute. She is an Associate Editor of the Journal of Shanghai University (Science edition). She is also a frequent reviewer for over ten scientific journals.

Josaphat Tetuko Sri Sumantyo (Senior Member, IEEE) was born in Bandung, Indonesia in 1970. He received the B.Eng. and M.Eng. degrees in electrical and computer engineering (subsurface radar systems) from Kanazawa University, Japan, in 1995 and 1997, respectively, and a Ph.D. degree in artificial system sciences (applied radio wave and radar systems) from Chiba University, Japan, in 2002.

From 2002 to 2005, he was a Lecturer (Postdoctoral Fellowship Researcher) with the Center for Frontier Electronics and Photonics, Venture Business Laboratory, Chiba University, Japan. From 2005 to 2013, he was an Associate Professor (permanent staff) with the Center for Environmental Remote Sensing, Chiba University, where he is currently a Full Professor (permanent staff). He is Head Department of Environmental Remote Sensing and Head Division of Earth and Environmental Sciences, Graduate School of Integrated Science and Technology, Chiba University in 2019-2020 and 2022-2023. Head of Disaster Information Analysis Research Division, Disaster Medical Research Center, Chiba University since 2021. He is also a lecturer in the Department of Electrical Engineering, Faculty of Engineering, Universitas Sebelas Maret (UNS), Indonesia since 2020. His research interest is theoretically scattering microwave analysis and its applications in microwave (radar) remote sensing, especially synthetic aperture radar, quantum radar, noise radar, and subsurface radar (VLF), including InSAR, DInSAR, and PS-InSAR, analysis and design of antennas for mobile satellite communications and microwave sensors, development of microwave sensors, including synthetic aperture radar for UAV, aircraft, high altitude platform system (HAPS), and microsatellite. He published about 930 journal and conference papers, and 15 book-related wave analyses, UAV, SAR, space antenna, and a small antenna. He is General Chair of the 7th and 8th Asia-Pacific Conference on Synthetic Aperture Radar (APSAR 2021 and 2023), and more than 290 Invited Talks and Lectures. He is Co-leader of the Technical Committee of Working Group on Remote Sensing Instrumentation and Technologies for UAV of IEEE-GRSS, Technical Committee on Instrumentation, and Future Technologies (IFT-TC), and Associate Editor of IEEE Geoscience and Remote Sensing Letter (GRSL) since 2021.

This work is licensed under a Creative Commons Attribution 4.0 License. For more information, see https://creativecommons.org/licenses/by/4.0/